UNIVERSITY OF BIRMINGHAM

Research at Birmingham

Biomechanical properties of human T cells in the process of activation based on diametric compression by micromanipulation

Du, Mingming; Kalia, Neena; Frumento, Guido; Chen, Frederick; Zhang, Zhibing

Link to publication on Research at Birmingham portal

Biomechanical properties of human T cells in the process of activation based on diametric compression by micromanipulation

Mingming Du[1], Neena Kalia[2], Guido Frumento[3,4], Frederick Chen[3,4]*, Zhibing Zhang [1,*]

[1] School of Chemical Engineering, University of Birmingham, Birmingham B15 2TT, UK

[2] Institute of Cardiovascular Sciences, University of Birmingham, Birmingham B15 2TT, UK

[3] Institute of Immunogy and Immunotherapy, University of Birmingham, Birmingham B15 2TT, UK

[4] NHS Blood and Transplant, Vincent Drive, Birmingham B15 2SG

*Authors for correspondence: Email: z.zhang@bham.ac.uk and frederick.chen@nhsbt.nhs.uk

Abstract

A crucial step in enabling adoptive T cell therapy is the isolation of antigen (Ag)-specific CD8$^+$ T lymphocytes. Mechanical changes that accompany CD8$^+$ T lymphocyte activation and migration from circulating blood across endothelial cells into target tissue, may be used as parameters for microfluidic sorting of activated CD8$^+$ T cells. CD8$^+$ T cells were activated in vitro using anti-CD3 for a total of 4 days, and samples of cells were mechanically tested on day 0 prior to activation and on day 2 and 4 post-activation using a micromanipulation technique. The diameter of activated CD8$^+$ T cells was significantly larger than resting cells suggesting that activation was accompanied by an increase in cell volume. While the Young's modulus value as determined by the force versus displacement data up to a nominal deformation of 10% decreased after activation, this may be due to the activation causing a weakening of the cell membrane and cytoskeleton. However, nominal rupture tension determined by compressing single cells to large deformations until rupture, decreased from day 0 to day 2, and then recovered on day 4 post-activation. This may be related to the mechanical properties of the cell nucleus. These novel data show unique biomechanical changes of activated CD8$^+$ T cells which may be further exploited for the development of new microfluidic cell separation systems.

Key words T lymphocytes; Activation; Cell Separation; Mechanics; Micromanipulation

Introduction

Cell-based therapies have witnessed tremendous expansion in the past two decades, from curative haematopoietic stem cell transplantation for leukemias to adoptive antigen (Ag)-specific CD8^{+} T cell immunotherapies of viral infections and cancers. CD8^{+} T cells for adoptive immunotherapies can be generated through *in vitro* expansion or immunomagnetic isolation of pre-existing Ag-specific lymphocytes from blood or tumor-infiltrating lymphocytes. The former method has the drawback of driving T cells to exhaustion through repeated cycles of *in vitro* antigen stimulation and expansion, which ultimately impacts on their efficacy to eliminate tumour or infected cells [1]. This is in contrast to direct *ex vivo* selection which requires minimal manipulation and thus retains the proliferative capacity and therapeutic functionality of the lymphocytes.

For this reason, immunomagnetic selection of fresh *ex vivo* cells has been adopted in recent clinical trials where a small number of pre-existing circulating virus-specific CD8^{+} T cells can be directly selected from donor blood to target viral infections and tumours in stem cell transplant patients [2-4]. This method has been used to treat cytomegalovirus, Epstein–Barr virus and adenovirus infections, and also lymphomas such as post-transplant lymphoproliferative disorder. Immunomagnetic selection systems utilize antibody or ligand-recognition of unique phenotypic markers on the cell surface to separate cells. With the recent breakthrough in utilising T cells expressing the CD19-specific chimeric antigen receptor (CAR) for the treatment of B cell acute lymphoblastic leukaemia [5], selection of Ag-specific cells could also become a key purification step in the *in vitro* expansion of immunoreceptor engineered cells.

71 However, there are limitations to immunomagnetic methods with regards to the loss of

72 low frequency cells through multiple processing steps such as washes and sub-optimal

73 purity and recovery from the selection itself, and not least, the costs of the specialized

74 GMP reagents. An alternate approach to immunomagnetic isolation, is to select cells

75 using clinical grade fluorescence-activated cell sorting (FACS) [6-8]. Though highly

76 sensitive and specific, FACS sorting of rare cells (<1%) to therapeutic quantities, is time

77 consuming and associated with the risk of reduced cell viability [9].

78

79 The biophysical properties of cells also allow different cell types to be discriminated. For

80 example, in flow cytometry the cell size determines light scattering properties, and in

81 apheresis, centrifugal forces separate blood into its constituent cellular components

82 based on physical properties. An emerging technique based on microfluidic separation

83 utilizes the biophysical properties of live cells by applying different hydrodynamic forces

84 on the target particles or by utilizing the natural biomechanical variation of the cells to

85 guide them into different flow paths [10]. Studies reporting cell sorting based on size or

86 stiffness demonstrate the potential applications of the microfluidic cell sorting technique

87 for separating tumor cells, erythrocytes as well as activated Ag-specific T cells [11-14].

88 It should therefore be possible to use natural or induced variations in biomechanical

89 properties to separate activated lymphocytes from non-activated lymphocytes and other

90 cell types.

91

92 However, before we can utilize microfluidic assays to separate lymphocytes for clinical

93 therapeutic purposes, a more precise study of their biomechanical properties is needed.

94   Parameters such as cell rigidity and deformability can be measured using several

95   techniques including atomic force microscopy (AFM), micromanipulation, magnetic

96   tweezers, micropipette aspiration, optical tweezers, shear flow, cell stretching and

97   microelectromechanical systems [15].   Powerful techniques such as AFM have

98   previously been used to measure the elastic properties of lymphocytes, but only deform

99   a portion of the cell surface (nano-indentation) and so do not measure the mechanical

100   properties of the whole cell [16]. However, circulating lymphocytes experience

101   significant repeated hydrodynamic and mechanical stresses in blood vessels, which are

102   applied along their entirety leading to large deformations in the microcirculation. These

103   are particularly seen following lymphocyte activation when they transmigrate out of

104   blood vessels into the surrounding interstitial tissue. Therefore, it is important to

105   understand the mechanical properties of lymphocytes under large, as well as small,

106   deformations.   Of the techniques mentioned, micromanipulation, based on the

107   compression of single cells between two parallel surfaces, can be used to generate

108   small to large deformations of cells, including deformations where they rupture, which is

109   appropriate for the purpose [17].

110

111   We report the first study that uses the micromanipulation technique to measure the

112   temporal biomechanical changes of CD8^{+} T cells following Ag-induced stimulation.

113   Moreover, the studies were conducted on live cells rather than fixed cells. We have

114   determined mechanical strength parameters such as rupture force, rupture deformation

115   and nominal rupture stress/tension for resting (unactivated) and activated T cells

116   compressed to rupture.   We have also modeled the compression data of T cells

117   corresponding to smaller deformations to obtain a measure of the elasticity, defined as

118   the Young's modulus. This work provides important new data on the biomechanics of

119   activated CD8$^+$ T cells which can be used for future development of microfluidic

120   separation of cells that have selectively responded to specific antigen stimulation.

121

122   **Materials and Methods**

123

124   **Isolation, culture and *in vitro* activation of T lymphocytes**

125

126   Peripheral blood was collected from three healthy drug-free adult donors after informed

127   consent. Peripheral blood mononuclear cells (PBMC) were isolated by Ficoll separation.

128   The contaminating erythrocytes were removed by osmotic lysis. Briefly, 1 ml of distilled

129   water was added to the cell pellet. After 30s, 14 ml of RPMI 1640 (Sigma-Aldrich, St.

130   Louis, MO, USA) was added, and the cells were washed once. Untouched CD8$^+$ T

131   lymphocytes were isolated by negative immunomagnetic selection, using CD8+ T Cell

132   Isolation Kit and LS columns (Miltenyi Biotec, Bergisch Gladbach, Germany), following

133   the manufacturer's instructions. Cell purity was checked using a FacsCanto II flow

134   cytometer (BD, San Jose, CA, USA) and in all the cases the CD8$^+$ T lymphocyte purity

135   was above 90%. Enriched CD8$^+$ T lymphocytes were resuspended in RPMI 1640 plus

136   10% foetal calf serum (Sigma-Aldrich, UK). Some cells were activated by culturing in

137   the presence of 30 ng/mL anti-CD3 antibody OKT3 (BioLegend, San Diego, CA, USA)

138   plus 600 U/mL IL-2 (Chiron, Emeryville, USA). For control samples, the non-activated

139 CD8$^+$ T cells were cultured in the medium for up to 4 days, and they were mechanically

140 tested on Day 0, Day 2 and Day 4.

141

142 **Micromanipulation technique**

143

144 The mechanical properties of resting and activated CD8$^+$ T lymphocytes were measured

145 either immediately after harvesting (day 0) or tested 2 days or 4 days post-activation.

146 Cells were diluted with phosphate buffered saline to reduce cell density in suspension

147 and mechanical testing was completed within 3 hours using a well established

148 micromanipulation technique, the principle and details of which have been previously

149 described [17, 18]. Briefly, the technique involves compression of a single cell between

150 the flat end of a probe and the bottom of a glass chamber containing the culture

151 medium (**Figure 1**). A microscopic image of a single mammalian cell under

152 compression is presented in [18]. Suspended single cells were allowed to settle to the

153 bottom of the chamber, and images were captured with a side-view high-speed digital

154 camera. A probe with a 25 μm diameter was driven down by a stepping motor towards

155 the single cells. The probe was connected to a force transducer (406A-ER, Aurora

156 Scientific Inc. Canada) in order to collect the data of instantaneous force imposed on

157 single cells at a frequency of 50 Hz.

158

159 **Determination of activation-related changes in cell size**

160

161 The diameter of CD8$^+$ T cells was directly measured from their images on a TV monitor

162 which was connected with the side view camera on the micromanipulation rig. The

163 magnification of the camera had been pre-calibrated, and the measurement of cell

164 diameter was accurate to ± 0.1μm. The cell size was also evaluated by flow cytometry.

165 The enriched CD8$^+$ T lymphocytes were stained with anti CD3/PE and 7AAD (BD). The

166 forward scatter (FSC-A) value of the 7AAD-/CD3+ cells was recorded using the

167 FacsCanto II flow cytometer (BD, San Jose, CA, USA).

168

169 **Determination of rupture force, rupture deformation, nominal rupture stress and**

170 **nominal rupture tension**

171

172 Single cells from each of the 3 donor samples were selected randomly and compressed

173 to large deformations until they ruptured using a probe at the speed of 2μm/s. The

174 numer of cells taken from each sample was 20 in order to give statistically

175 representative results. The force (μN) imposed on the cell was plotted against the

176 distance (μm) the probe moved towards the glass chamber (force vs displacement).

177 These graphs were then used to determine the mean rupture force and the percentage

178 (%) deformation at rupture for resting and activated cells. The % rupture deformation

179 was calculated as the ratio of the displacement value at rupture to the initial diameter of

180 the cell.

181

182 Nominal rupture stress (σ_R) was calculated as the ratio of the rupture force to the initial

183 cross-sectional area of the cell. Nominal rupture tension (T_R) was calculated as the

184 ratio of the rupture force to the initial diameter of the cell. These values provide a

185 comparable indication of the mechanical strength of cells and were calculated using

186 Equations (1) and (2) respectively, where F_R is the rupture force and *d* is the original

187 diameter of the single cell before compression.

188

189 $$\sigma_R = \frac{4F_R}{\pi d^2} \qquad\qquad (1)$$

190 $$T_R = \frac{F_R}{d} \qquad\qquad (2)$$

191

192 **Determination of the Young's Modulus**

193 Theoretically, the Hertz model is valid and commonly used to describe the relationship

194 between the imposed force and displacement for small deformations of an elastic

195 object, which has been successfully applied to determination of the Young's Modulus of

196 different particles including cells when compressed to a small deformation [19-21]. The

197 experimental force versus displacement data up to a nominal deformation of 10% were

198 fitted to Equation (3), similar to the approach described in [20] to determine the Young's

199 modulus of T cells, having presumed that the individual cells were homogeneous,

200 incompressible, elastic spheres and that there was no friction at the cell-substrate

201 interfaces.

$$202 \quad F = \frac{E^*\sqrt{2R}}{3(1-\upsilon^2)}\delta^{3/2} \qquad\qquad (3)$$

203   where F is the applied force, E is the Young's modulus of the cell, R is the original cell

204   radius, ν is the Poisson's ratio of the cell and δ is the diametric compressive

205   displacement. From the model, there should be a linear relationship between F and $\delta^{3/2}$.

206   From the slope of the linear fitting, cell radius and Poisson ratio (assumed to be 0.5

207   since the cells are assumed to be incompressible), the value of Young's modulus was

208   determined - higher values indicate cells that are less deformable for a given applied

209   force and vice versa.

210

211   **Statistical analysis**

212   Values for the mechanical property parameters of the lymphocytes are presented as

213   mean ± standard error. Paired Student t-tests were performed to determine significant

214   differences among the mechanical properties of different samples, with statistical

215   significance reported at the 95% confidence level (p<0.05).

216

217   **Results**

218   **Activation of CD8⁺ T lymphocytes increases their cell size**

219   The diameter of the single cells was measured from their images using the side-view

220   camera on the micromanipulator. The diameter of resting CD8+ T cells (day 0) was 6.1

221   ± 0.6 µm. This increased significantly ($p < 0.05$) upon activation to 9.7 ± 1.1 µm on day 2

222   post-activation and remained significantly ($p < 0.05$) greater on day 4 post-activation

223   when compared to resting cell values (**Figure 2a)**. There was no significant difference

224   between the activated samples at day 2 and day 4 post-activation. Changes in cell

225   diameter are also shown by the data generated using flow cytometry (**Figure 2b**). The

226   FSC-A value of resting T cells are again significantly greater on day 2 ($p < 0.05$) and day

227   4 post-activation ($p < 0.05$) when compared to resting cell values. Interestingly, it was

228   noted that CD8+ T cells that had been activated and tested on day 2 post-activation

229   tended to 'stick' to the force transducer probe (image not shown), possibly indicating

230   some change in their adhesive nature in the early stages of activation.

231

232   **Compression curves of T cells to rupture**

233   Micromanipulation studies demonstrated that the individual CD8+ T cells tested in the

234   same sample were heterogeneous in their diameter and their force versus displacement

235   curves even for single cells of same diameter, however, all tested single cells showed

236   common characteristics in their compression curves. Typical curves showing the

237   relationship between the force and displacement during continuous diametrical

238   compression of a single lymphocyte to rupture at day 0, 2 and 4 days post-activation are

239   shown in **Figures 3a-c**. At point A, the probe started to touch the cell, and the resistant

240   force increased until point B where the cell ruptured. As a result of rupture, the force

241 decreased rapidly to point C, followed by curve CD where the force increased

242 continuously which represents the compression of cell debris until the probe touched

243 bottom of the glass chamber.

244

Rupture force increases at 4 days post-activation

245

246 The mean cell rupture force (μN) was determined from the force vs displacement curves

247 (*y*-axis value at point B). The rupture force was similar between the resting (day 0) and

248 activated cells at 2 days post-activation with mean values of 2.3 ± 0.8 µN and 2.6 ± 0.9

249 µN respectively. However, when activated cells were analyzed at 4 days, the rupture

250 force significantly (p<0.05) increased to 4.6 ± 1.6 µN (p<0.05) when compared to resting

251 cells (**Figure 4a**). The % rupture deformations of resting T lymphocytes and activated

252 lymphocytes at 2 and 4 days post-activation was not significantly different with mean

253 values of 78.3 ± 1.3%, 79.7 ± 1.6% and 77.5 ± 1.5% obtained respectively (**Figure 4b**).

254

Nominal rupture stress / tension decreases at 2 days post-activation

255

256 The nominal rupture tension significantly (p<0.05) decreased from 0.58 ± 0.07 N/m for

257 resting cells to 0.45 ± 0.07 N/m for cells at 2 days post-activation. This increased to

258 0.62 ± 0.10 N/m on day 4 post-activation, a value not significantly different to resting

259 cells (**Figure 5**). A similar pattern was observed for nominal rupture stress (**Figure 5**).

260

261 **Young's modulus decreases in activated CD8$^+$ T cells**

262 The Young's modulus was calculated from data obtained corresponding to small

263 deformations of T cells. Typical force versus displacement data with a linear fit based on

264 the Hertz model for cells at day 0, 2 and 4 days post-activation are shown in **Figures**

265 **6a-c**. Mean correlation coefficient values of 0.84 ± 0.05, 0.85 ± 0.04 and 0.85 ± 0.06 were

266 obtained for resting cells and cells at 2 days post-activation and 4 days post-activation

267 respectively. The values of Young's modulus decreased significantly at both 2 days

268 post-activation ($p<0.05$) and 4 days post-activation ($p<0.05$) when compared to resting

269 cells at day 0 (**Figure 6d**). Actual calculated mean values for the Young's Modulus

270 were 58.0 ± 6.3 kPa, 43.7 ± 5.0 kPa, and 43.0 ± 6.3 kPa for T lymphocytes at day 0, day

271 2 post-activation and day 4 post-activation respectively. There was no significant

272 difference in the mean Young's modulus between T cells activated for 2 days and 4

273 days ($p>0.05$).

No change in the mechanical properties of non-activated CD8+ T cells for up to 4 days

276 The diameter of non-activated T cells did not change significantly upon incubation on

277 day 2 and day 4 when cultured in the medium (Figure 7a). There was also no significant

278 difference in the nominal rupture tension/stress between the resting samples, as shown

279 in Figure 7b.

Discussion

281 This novel study analysed the biomechanical properties of live lymphocytes undergoing

282 activation using a micromanipulation technique, without the need for fixing the cells.

283　Mammalian cells can show heterogeneity in their biomechanical property parameters,

284　which is reflected in the standard error of the mean, and 3 donors should give

285　reasonably representative results [22]. An increase in cell volume was observed as a

286　result of activation at both 2 and 4 days post-activation. An initial fall in whole cell

287　mechanical strength was observed at 2 days post-activation as indicated by the

288　decreased rupture stress/tension values. Thereafter, although lymphocytes remained

289　bigger, they regained their mechanical strength at day 4 post-activation, possibly

290　reflecting the tailing off of activation and cellular recovery.　However, the Young's

291　modulus at small deformations (up to 10%), decreased at both 2 and 4 days post-

292　activation suggesting the outer membrane became and remained flexible. This is the

293　first time, as far as we are aware, that a micromanipulation technique has been used to

294　directly analyze the biomechanical properties including rupture strength of human T

295　cells at various time points post-activation. A summary of the data obtained are

296　provided in Table 1 below.

297

298　Table 1: Change in the mechanical properties of human T cells at 2 days and 4 days

299　post-activation

All values compared to resting cells	Cell size	Rupture force	% rupture deformation	Rupture stress and tension	Young's modulus
2 days post-activation	↑	–	–	↓	↓
4 days post-activation	↑	↑	–	–	↓

300

301

The rupture force for activated cells at 4 days post-activation was significantly greater than resting and activated cells at 2 days post-activation. At first glance, this suggested these cells were "stronger", thus requiring the greater force to rupture. However, this data did not take into account that the size of the cells was different for the three groups which could explain their differing rupture force. Increases in CD8+ T cell size at similar time points have previously been described microscopically post-OKT3 activation [23, 24] and occurs so that activated lymphocytes can duplicate their contents and divide. To make comparisons between the mechanical properties of resting and activated cells, nominal rupture stress and tension was calculated, which took into account the initial cross-sectional area and diameter of the cells. It should be pointed out that the initial cross-sectional area may be different from the real contact area between the force probe or bottom substrate and cell at rupture, and the latter depends on the deformation at rupture. As Figure 3b shows, the deformation at rupture did not change significantly up to 4 days, the choice of using nominal rupture stress for comparison is still valid. Once corrected for size, it became apparent that resting cells and cells at 4 days post-activation were equally strong but more than cells at 2 days post-activation. Hence the nominal stress/tension data indicated that CD8$^+$ T lymphocytes became weaker early during activation, while their mechanical strength was regained 4 days later. The higher mechanical strength of the resting lymphocytes is essential functionally to maintain sufficient integrity and thus protect them from damage by the significant hydrodynamic and mechanical stresses exerted on them in the circulation [25]. Following stimulation by Ag-presenting cells *in vivo*, CD8+ T cells move out of the circulation to the site of

324 infection where they acquire cytolytic effector activity against the pathogen. Therefore,

325 the initial weakened cellular strength observed in this study may functionally correlate

326 with, and enable, the transmigration of circulating lymphocytes between endothelial

327 cells into tissue. After this event, lymphocytes regain their original form and strength for

328 mediating effector activity and this functionally correlates with the higher nominal

329 rupture stress/tension observed at 4 day post-activation than day 2.

330

331 Previous studies have shown that the nucleus of T lymphocytes is approximately 5

332 times stiffer than the cytoplasm and occupies about 80% of the cell [26]. This

333 characteristic makes T lymphocytes different from other eukaryocyte cells

334 (mesenchymal cells, endothelial cells, etc.) in which the cell nucleus only occupies

335 ~10% of the cell volume [27]. When faced with higher compressive forces, the

336 lymphocyte cell nucleus therefore plays an increasingly significant role in resisting the

337 applied force for the whole cell. The reduced nominal rupture stress / tension at 2 days

338 post-activation indicates the cell nucleus, as well as the cell membrane and

339 cytoskeleton of these larger cells, may have become less strong. However, at the later

340 stage of activation (from day 2 to day 4), these structures regained their mechanical

341 strength while cell volume remained unchanged during this time.

342

343 At lower applied force, which compresses the cell to a smaller deformation, the

344 mechanical stiffness of T cells is governed primarily by the membrane which is

345 considered to be largely elastic. The Young's modulus is a measure of the intrinsic

346 stiffness of an elastic material undergoing recoverable compression. The Hertz model

347 was able to determine the Young's modulus of T lymphocytes at small deformations (up

348 to 10%), hence providing an indication of the elasticity of the outer region (cell

349 membrane and cytoskeleton) of the cell. Although the noise to signal ratio is relatively

350 big corresponding to small deformations, significant differences between samples were

351 still demonstrated from the values of Young's Modulus. The results indicate that

352 depolymerization or reorganization of cytoskeleton polymers probably happened when

353 the cells were activated, resulting in softness of the outer cortex during the 4 days. From

354 the rupture parameters at large deformation and the Young's Modulus calculated at

355 small deformation, we hypothesized that the cytoskeleton remained less stiff post-

356 activation, while the nucleus regained rigidity during the 4 days activation, which

357 remains to be validated in future. In the calculation of Young's modulus, for living cells,

358 the Poisson ratio is typically between 0.4 and 0.5, which means they are mostly or fully

359 incompressible [28]. A value of 0.5 is chosen here since the Poisson ratio of $CD8^+$ T

360 lymphocytes has not been studied. Moreover, from the Hertz model (Eq. 3), it can be

361 seen that Poisson ratio (v) has little effect on Young's modulus that increases by only

362 12% when v varies from 0.4 to 0.5. For measuring the local Young's modulus of the cell

363 membrane with greater sensitivity, and its spatial distribution, AFM may be used which

364 can measure the forces in the order of pico-Newton to nano-Newton.

365

366 **Conclusions**

367

368 Using biomechanical properties in microfluidic cell sorting is increasingly recognized as

369 a marker-free way to separate biological cells. With the increasing interest in using

370 CD8+ T cells for therapeutic purposes, a separation method in which cells remain

371 unperturbed is important if they are to be transplanted after mechanical characterization

372 and sorting.   This study utilizes the micromanipulation technique, a relatively

373 straightforward method to evaluate the mechanical property changes of activated CD8+

374 T lymphocytes. It has been found that there was no significant change in the

375 mechanical property parameters including cell size, nominal rupture stress and rupture

376 tension of non-activated CD8+ T cells in the culture medium for up to 4 days, which is in

377 clear contrast to those activated in vitro using anti-CD3. The activated cells showed a

378 significant increase in size and decrease in rupture stress/tension at day 2 but the

379 mechanical strength recovered at day 4.The data obtained on size and mechanical

380 properties post-activation may be utilized for developing microfluidic devices for their

381 separation. Furthermore, this work obtains complementary data for CD8+ T cells

382 circulating *in vivo* with respect to adapting to the mechanical barriers. The ability to

383 directly measure the biomechanical properties of live lymphocyte subsets not only

384 facilitates the development of a cell separation system based on defined physical

385 properties of cells but also provides a 'biomarker' for assessing the physical state of

386 lymphocytes, that could be used for assessing quality after bioprocessing of cells eg.

387 cryopreservation.

388

389 .

390

391

Acknowledgments

395

References

[1] Klebanoff CA, Gattinoni L, Restifo NP. Sorting through subsets: Which T cell populations mediate highly effective adoptive immunotherapy? J Immunol 2012;35:651.

[2] Peggs KS, Verfuerth S, Pizzey A, Khan N, Guiver M, Moss PA, et al. Adoptive cellular therapy for early cytomegalovirus infection after allogeneic stem-cell transplantation with virus-specific T-cell lines. The Lancet. 2003;362:1375-7.

[3] Feuchtinger T, Matthes-Martin S, Richard C, Lion T, Fuhrer M, Hamprecht K, et al. Safe adoptive transfer of virus-specific T-cell immunity for the treatment of systemic adenovirus infection after allogeneic stem cell transplantation. Br J Haematol 2006;134:64-76.

[4] Moosmann A, Bigalke I, Tischer J, Schirrmann L, Kasten J, Tippmer S, et al. Effective and long-term control of EBV PTLD after transfer of peptide-selected T cells. Blood. 2010;115:2960-70.

[5] Davila ML, Riviere I, Wang X, Bartido S, Park J, Curran K, et al. Efficacy and toxicity management of 19-28z CAR T cell therapy in B cell acute lymphoblastic leukemia. Sci Transl Med 2014;6:224ra25-ra25.

[6] Cepok S, Zhou D, Srivastava R, Nessler S, Stei S, Büssow K, et al. Identification of Epstein-Barr virus proteins as putative targets of the immune response in multiple sclerosis. J Clin Invest 2005;115:1352-1360.

[7] Kodituwakku AP, Jessup C, Zola H, Roberton DM. Isolation of antigen-specific B cells. Immunol Cell Biol 2003;81:163-70.

[8] Sung J, Yang H-M, Park J, Choi G-S, Joh J-W, Kwon C, et al. Isolation and characterization of mouse mesenchymal stem cells. Transplant Proc 2008; 40:2649-54.

[9] Wulff S, Martin K, Vandergaw A, Boenisch T, Brotherick I, Hoy T, et al. DakoCytomation - Guide to Flow Cytometry. 2006.

[10] Tsutsui H, Ho C-M. Cell separation by non-inertial force fields in microfluidic systems. Mech Res Commun 2009;36:92-103.

[11] Lim CT, Hoon DSBH. Circulating tumor cells: Cancer's deadly couriers. Physics Today 2014; 67: 26-30..

[12] Hou HW, Bhagat AAS, Chong AGL, Mao P, Tan KSW, Han J, et al. Deformability based cell margination—a simple microfluidic design for malaria-infected erythrocyte separation. Lab Chip 2010;10:2605-13.

[13] Hur SC, Henderson-MacLennan NK, McCabe ER, Di Carlo D. Deformability-based cell classification and enrichment using inertial microfluidics. Lab Chip 2011;11:912-20.

[14] Preira P, Grandne V, Forel J-M, Gabriele S, Camara M, Theodoly O. Passive circulating cell sorting by deformability using a microfluidic gradual filter. Lab Chip 2013;13:161-70.

[15] Neubauer MP, Poehlmann M, Fery A. Microcapsule mechanics: From stability to function. Adv Colloid Interface Sci 2014;207:65-80.

[16] Cai X, Xing X, Cai J, Chen Q, Wu S, Huang F. Connection between biomechanics and cytoskeleton structure of lymphocyte and Jurkat cells: An AFM study. Micron. 2010;41:257-62.

[17] Nguyen BV, Wang QG, Kuiper NJ, El Haj AJ, Thomas CR, Zhang Z. Biomechanical properties of single chondrocytes and chondrons determined by micromanipulation and finite-element modelling. J R Soc Interface 2010;7:1723-33.

438 [18] Nguyen BV, Wang Q, Kuiper NJ, El Haj AJ, Thomas CR, Zhang Z. Strain-dependent
439 viscoelastic behaviour and rupture force of single chondrocytes and chondrons under
440 compression. Biotechnol Lett 2009;31:803-9.
441 [19] Kuznetsova TG, Starodubtseva MN, Yegorenkov NI, Chizhik SA, Zhdanov RI. Atomic
442 force microscopy probing of cell elasticity. Micron 2007;38:824-33.
443 [20] Yan Y, Zhang Z, Stokes JR, Zhou Q-Z, Ma G-H, Adams MJ. Mechanical characterization
444 of agarose micro-particles with a narrow size distribution. Powder Technol 2009;192:122-30.
445 [21] Martens JC, Radmacher M. Softening of the actin cytoskeleton by inhibition of myosin II.
446 Pflugers Arch, EJP 2008;456:95-100.
447 [22] Pleumeekers MM, Nimeskern L, Koevoet WLM, Kops N, Poublon RML, Stok KS, van
448 Osch GJVM. The in vitro and in vivo capacity of culture-expanded human cells from several
449 sources encapsulated in alginate to form cartilage. Eur Cell Mater 2014; 27: 264-280.
450 [23] Wu Y, Lu H, Cai J, He X, Hu Y, Zhao H, et al. Membrane surface nanostructures and
451 adhesion property of T lymphocytes exploited by AFM. Nanoscale Res Lett 2009;4:942-7.
452 [24] Teague TK, Munn L, Zygourakis K, McIntyre BW. Analysis of lymphocyte activation and
453 proliferation by video microscopy and digital imaging. Cytometry 1993;14:772-82.
454 [25] Brown MJ, Hallam JA, Colucci-Guyon E, Shaw S. Rigidity of circulating lymphocytes is
455 primarily conferred by vimentin intermediate filaments. J Immunol 2001;166:6640-6.
456 [26] Friedl P, Wolf K, Lammerding J. Nuclear mechanics during cell migration. Curr Opin Cell
457 Biol 2011;23:55-64.
458 [27] Tsien R, Pozzan T, Rink T. Calcium homeostasis in intact lymphocytes: cytoplasmic free
459 calcium monitored with a new, intracellularly trapped fluorescent indicator. J Cell Biol
460 1982;94:325-34.
461 [28] Trickeya WR, Baaijensb FPT, Laursenc TA, Alexopoulosa LG, Farshid Guilaka F.
462 Determination of the Poisson's ratio of the cell: recovery properties of chondrocytes after release
463 from complete micropipette aspiration. J Biomech 2006; 39:78–87.
464
465

466

467

468

469

470

471

Figure Legends

474 **Figure. 1.** Schematic diagram of the micromanipulation rig: (1) Force transducer; (2)

475 probe; (3) stepping motor; (4) computer with motor control and data acquisition system;

476 (5) Bottom-view microscope; (6) side-view microscope; (7) high-speed camera; (8)

477 single cells in phosphate buffered saline; (9) glass chamber.

478 **Figure 2.** Changes in the diameter of T lymphocytes was quantitated using (a) direct

479 measurement of a microscopy image generated using the side-view camera on the

480 micromanipulator and (b) flow cytometry. Both methods showed a similar significant

481 increase in cell diameter as a result of T cell activation. N=3 donor samples for each

482 group with 20 single cells, selected randomly from each sample. *p<0.05 as determined

483 using a paired Student t-test.

484 **Figure 3.** Typical force-displacement curves obtained at a compression speed of 2µm/s

485 for T cells to rupture on (a) day 0 prior to activation (resting cells) (b) day 2 post-

486 activation and (c) day 4 post-activation. At point A, the probe touched the cell and the

487 resistant force increased until point B where the cell ruptured. Rupture resulted in the

488 force decreasing rapidly to point C, followed by curve CD where force increased until

489 the probe touched bottom of the glass chamber. N=3 donor samples for each group

490 with 20 single cells, selected randomly from each sample. *p<0.05 as determined using

491 a paired Student t-test.

492   **Figure 4.** The (a) mean rupture force and (b) mean rupture deformation of T cells on (a)

493   day 0 prior to activation (resting cells) (b) day 2 post-activation and (c) day 4 post-

494   activation. The force required to rupture cells was larger for activated cells at 4 days

495   post-activation. All cells were ruptured when they reached a % deformation close to

496   80%. N=3 donor samples for each group with 20 single cells, selected randomly from

497   each sample. *$p<0.05$ as determined using a paired Student t-test.

498   **Figure 5.** The nominal rupture tension and nominal rupture stress of T cells on (a) day 0

499   prior to activation (resting cells) (b) day 2 post-activation and (c) day 4 post-activation.

500   Both values significantly decreased for cells at 2 days post-activation. N=3 donor

501   samples for each group with 20 single cells, selected randomly from each sample.

502   *$p<0.05$ as determined using a paired Student t-test.

503   **Figure 6.** The typical linear fit (line) of the Hertz model to the obtained force-

504   displacement data (o) for T cells compressed to small deformations on (a) day 0 prior

505   to activation (resting cells) (b) day 2 post-activation and (c) day 4 post-activation. The

506   mean values of the correlation coefficient are 0.84±0.05, 0.85±0.04 and 0.85±0.06

507   respectively with an overall range of 0.7 to 0.9. (d) The Young's modulus was

508   calculated from these data, which decreased significantly as a results of activation. N=3

509   donor samples for each group with 20 single cells, selected randomly from each

510   sample. *$p<0.05$ as determined using a paired Student t-test.

511
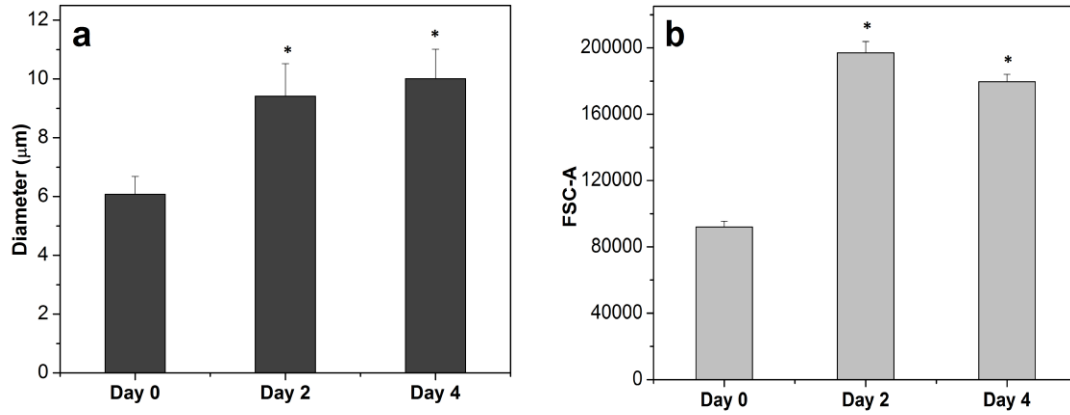
512

513   FIGURE 1
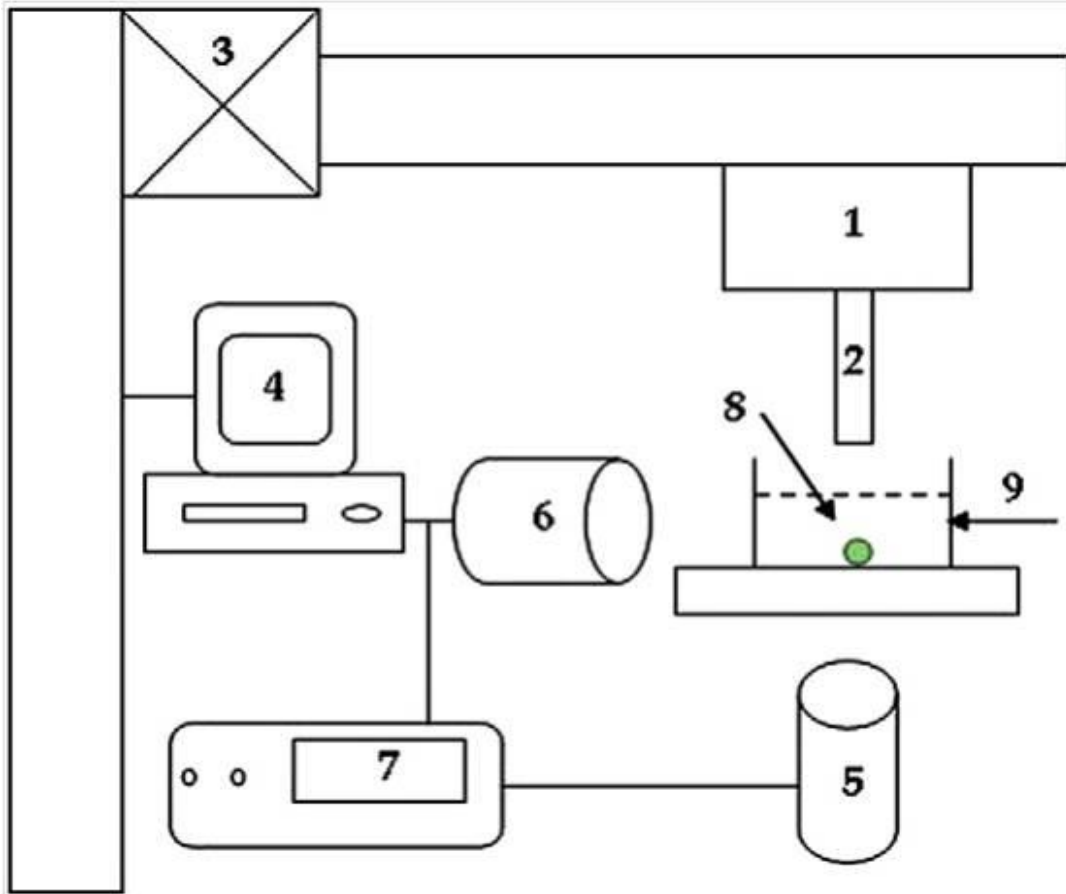
514

515

516

517

518

519

520

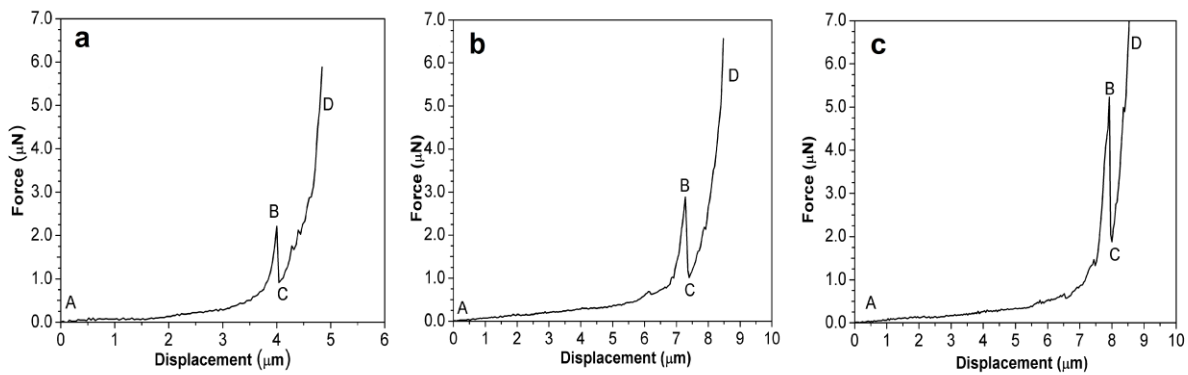521 FIGURE 2

522

523

524

525

526

527

528

529

530

531
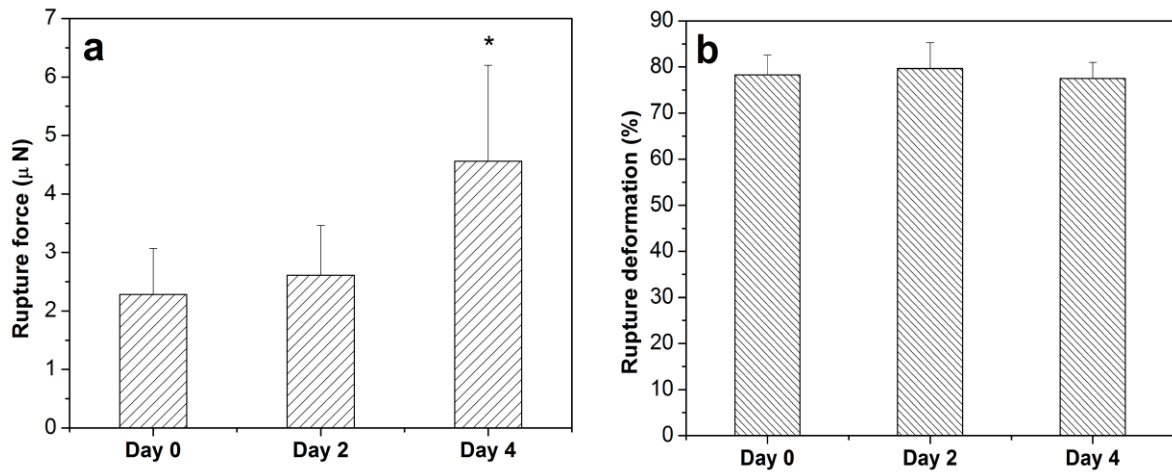
532

533   FIGURE 3

545   FIGURE 4

546

547

548

549

550

551

552

553

554

555
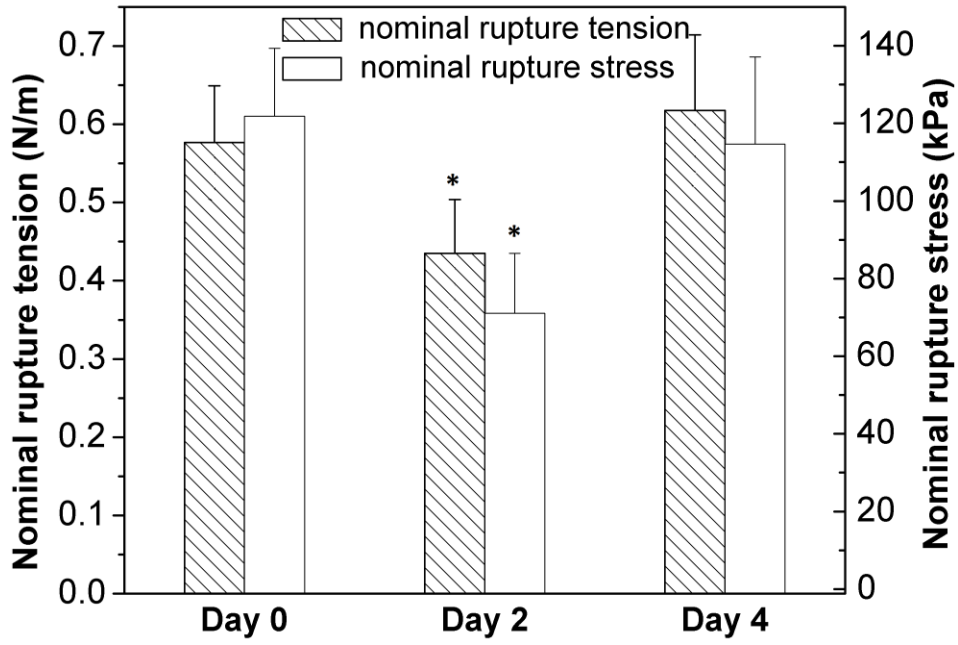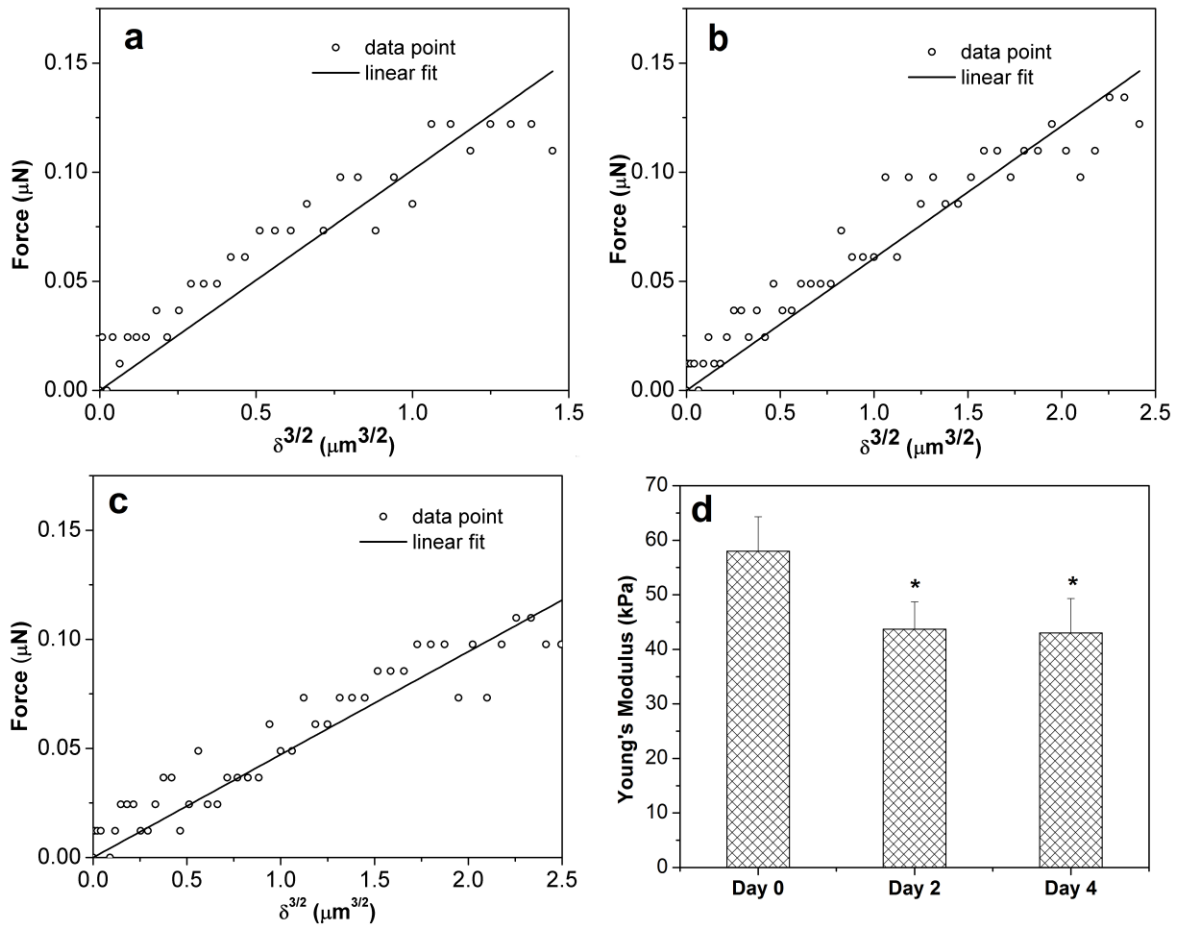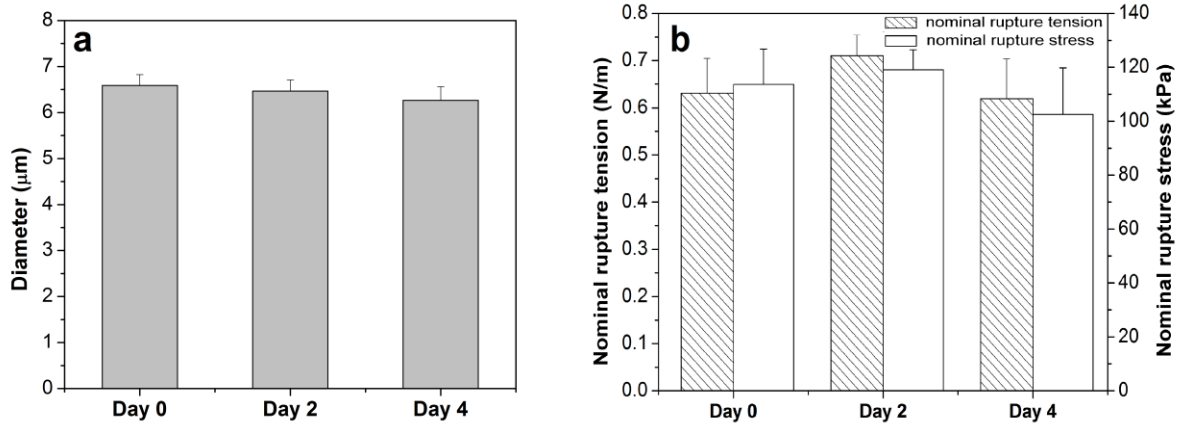
557

558

559

560

561

562

563

564

565   FIGURE 6

566

567

568

569

570

571

572   FIGURE 7

573